LA-UR-

Approved for public release;
distribution is unlimited.

Title:	**QUIC-PLUME Theory Guide** ***(Version 5.5)***
Author(s):	Michael D. Williams Michael J. Brown Matthew A. Nelson
Intended for:	Public Distribution March 16, 2009

Form 836 (7/06)

Table of Contents

1. Introduction

The Quick Urban & Industrial Complex (QUIC) Dispersion Modeling System is intended for applications where dispersion of airborne contaminants released near buildings must be computed quickly. Fast-running models are essential for vulnerability studies where many cases must be simulated in a limited amount of time or for emergency response scenarios when an answer is needed quickly. However, the dispersion of an airborne contaminant released in an urban area is difficult to predict due to the presence of buildings. Traditional fast-running dispersion models currently in use have little or no building "awareness".

The QUIC fast-response urban dispersion modeling system computes three-dimensional wind patterns and dispersion of airborne contaminants around clusters of buildings. QUIC can run on a laptop and provide results in tens of seconds to tens of minutes depending on the problem size. QUIC is intended to complement Gaussian puff/plume models and full-physics computational fluid dynamics (CFD) models, being more accurate than the former and much faster than the latter. QUIC will never give perfect answers, but it will account for the bulk effects of buildings and provide more realism than non-building aware dispersion models.

QUIC is composed of the QUIC-URB wind solver, the QUIC-PLUME dispersion model, the QUIC-PRESSURE pressure solver, and a graphical user interface, QUIC-GUI. An official use only version of the code has been adapted for chemical, biological, and radiological (CBR) agent transport and dispersion problems. This document describes the basic QUIC-PLUME model equations, the special considerations needed for urban applications, and assumptions made in the turbulence parameterizations. In addition, new schemes that have been added since the 2004 version of the QUIC-PLUME Theory Guide are described, including explosive buoyant rise, dense gas, tree canopy turbulence, and outdoor-to-indoor infiltration schemes. Companion documents describe the QUIC-URB model (Pardyjak and Brown, 2003), how to run QUIC-PLUME in standalone mode (Williams et al., 2004), and how to use the QUIC-GUI (Nelson et al., 2007). Validation studies are found in, e.g., Brown et al. (2009), Allwine et al. (2008), Gowardhan et al. (2008), Singh et al. (2008), Gowardhan et al. (2007), Bowker et al. (2007a, b), Senocak et al. (2007), Favaloro et al. (2007), Bowker et al. (2004), Williams et al. (2004).

2. Model Overview

Buildings produce complex flows that pose difficult challenges to dispersion modelers. The QUIC-URB model uses an empirical-diagnostic approach based on Röckle (1990) to compute a mass consistent 3D wind field around buildings. The QUIC-PLUME model is a Lagrangian dispersion model that uses the mean wind fields from QUIC-URB and turbulent winds computed internally using the Langevin random walk equations. Gradient-based and non-local mixing turbulence schemes are used to estimate the turbulence parameters.

The QUIC-PLUME code does not use the traditional two- or three-term random-walk equations that have been used successfully for boundary-layer flow problems (e.g., Wilson et al., 1981; Ley, 1982; Anfossi et al, 1998; Hurley et al, 2005). As shown by Thomson (1987), when the mean flow and Reynolds stresses are spatially variable more terms are needed in the random-walk equations to satisfy the well-mixed criterion. Due to the horizontal inhomogeneity of the flow around buildings, the QUIC-PLUME code contains additional terms and a unique coordinate rotation approach is used in order to account for lateral and vertical mean motions and horizontal gradients in turbulence parameters. Details of the QUIC-PLUME model formulation follow.

3. Random-Walk Model Equations

Lagrangian random-walk models describe dispersion by simulating the releases of tagged fluid parcels or aerosol particles and move them with an instantaneous wind composed of a mean wind plus a turbulent wind (see Rodean, 1996). Note that in this document we will call the tagged airborne contaminant “marker particles”, but realize that these markers represent both gases and true particles with aerodynamic diameter d. The equations that describe the positions of these marker particles are:

$$x(t+\Delta t) = x(t) + \overline{U}\Delta t + u'(t)\Delta t,$$

$$y(t+\Delta t) = y(t) + \overline{V}\Delta t + v'(t)\Delta t,$$

and

$$z(t+\Delta t) = z(t) + \overline{W}\Delta t + w'(t)\Delta t,$$

where *x, y,* and *z* are the current position coordinates of the particle in the east-west, north-south, and vertical directions, respectively, $\overline{U}$, $\overline{V}$, and $\overline{W}$ are the mean winds and u', v', and w' are the fluctuating components of the instantaneous wind in the x, y, and z directions, respectively, and Δt is the time step.

The mean winds are computed by the QUIC-URB or QUIC-CFD wind solvers, while the fluctuating components of the instantaneous winds are calculated from:

$$u'(t+\Delta t) = u'(t) + du',$$

$$v'(t+\Delta t) = v'(t) + dv',$$

and

$$w'(t+\Delta t) = w'(t) + dw'.$$

Mean winds are interpreted as averaged over a sufficient length of time (usually 10 minutes to an hour) to remove the effects of quasi-random fluctuations.

Thomson's (1987) solution that supports the "well-mixed" criterion is:

$$dU_i = -\frac{C_o\varepsilon}{2}\sum_{k=1}^{3}\lambda_{ik}\left(U_k-\overline{U}_k\right)dt + \sum_{j=1}^{3}\overline{U}_j\frac{\partial\overline{U}_i}{\partial x_j}dt + \sum_{j=1}^{3}\left[\frac{\partial\overline{U}_i}{\partial x_j} + \sum_{m=1}^{3}\frac{\lambda_{im}}{2}\sum_{k=1}^{3}\overline{U}_k\frac{\partial\tau_{km}}{\partial x_j}\right]\left(U_j-\overline{U}_j\right)dt +$$
$$\sum_{m=1}^{3}\frac{\lambda_{im}}{2}\sum_{k=1}^{3}\sum_{j=1}^{3}\frac{\partial\tau_{km}}{\partial x_j}\left(U_j-\overline{U}_j\right)\left(U_k-\overline{U}_k\right)dt + \frac{1}{2}\sum_{j=1}^{3}\frac{\partial\tau_{ij}}{\partial xj}dt + (C_o\varepsilon dt)^{1/2}d\Omega_i(t),$$

where dU_i is the change of the instantaneous wind over a time increment dt, U_i is the instantaneous wind, τ_{ij} is the kinematic Reynolds stress tensor, and $\lambda_{im} = \tau_{im}^{-1}$ (see also Rodean, 1996). The terms with the gradients of the Reynold's shear and normal stress are called the drift terms and act to inhibit collection of particles in pockets of low turbulence (e.g., near walls).

Dramatic simplifications can be made to this equation if the mean vertical wind $\overline{W}$ is zero, the coordinate system is rotated so that the mean wind is in the x-direction ($\overline{V} = 0$), and the mean wind and turbulence statistics are spatially invariable in the horizontal and quasi-stationary. Under these circumstances, the expressions for the incremental changes in the turbulent velocity fluctuations are:

$$du' = \frac{-C_o\varepsilon}{2}\left[\lambda_{11}u' + \lambda_{13}w'\right]dt + \frac{1}{2}\frac{\partial\tau_{13}}{\partial z}dt + \frac{1}{2}\frac{\partial\tau_{11}}{\partial z}\left[\lambda_{11}u'w' + \lambda_{13}w'^2\right]dt + \frac{1}{2}\frac{\partial\tau_{13}}{\partial z}\left[\lambda_{13}u'w' + \lambda_{33}w'^2\right]dt + \left(C_o\varepsilon dt\right)^{1/2}d\Omega_1(t),$$

$$dv' = -\frac{C_o\varepsilon}{2}\lambda_{22}v'dt + \frac{1}{2}\frac{\partial\tau_{22}}{\partial z}\lambda_{22}v'w'dt + \left(C_o\varepsilon dt\right)^{1/2}d\Omega_2(t),$$

and,

$$dw' = -\frac{C_o\varepsilon}{2}\left[\lambda_{13}u' + \lambda_{33}w'\right]dt + \frac{1}{2}\frac{\partial\tau_{33}}{\partial z}dt + \frac{1}{2}\frac{\partial\tau_{13}}{\partial z}\left[\lambda_{11}u'w' + \lambda_{13}w'^2\right]dt + \frac{1}{2}\frac{\partial\tau_{33}}{\partial z}\left[\lambda_{13}u'w' + \lambda_{33}w'^2\right]dt + \left(C_o\varepsilon dt\right)^{1/2}d\Omega_3(t),$$

where $\lambda_{11} = \left(\tau_{11} - \frac{\tau_{13}^2}{\tau_{33}}\right)^{-1}$, $\lambda_{22} = \tau_{22}^{-1}$, $\lambda_{33} = \left(\tau_{33} - \frac{\tau_{13}^2}{\tau_{11}}\right)^{-1}$, $\lambda_{13} = \left(\tau_{13} - \frac{\tau_{11}\tau_{33}}{\tau_{13}}\right)^{-1}$,

$$\tau_{11} = \sigma_u^2,\ \tau_{22} = \sigma_v^2,\ \tau_{33} = \sigma_w^2 \text{ and } \tau_{13} = \overline{u'w'}.$$

The constant C_o is called the universal constant for the Lagrangian structure function. A variety of investigators have estimated values for C_o ranging from 1.6 to 10 and we have chosen a value of 5.7 based on Rodean (1996). ε is the mean rate of turbulence kinetic energy dissipation. $d\Omega_1(t)$, $d\Omega_2(t)$, and $d\Omega_3(t)$ are uncorrelated, normally distributed random variables with means of zero and standard deviations of one. Note that we have converted the equations to be in terms of the fluctuating velocities using the derivations described by Weil (2005) in which the relationship $dU_i = d\overline{U}_i + du_i'$ is used.

For the first time step, the initial values of u', v', and w' are given by:

$$u'(t_0) = \sigma_u d\Omega_1,$$

$$v'(t_0) = \sigma_v d\Omega_2,$$

and,

$$w'(t_0) = \sigma_w d\Omega_3.$$

a) Coordinate Rotation to Better Account for Urban Flows

Although the above formulation is an improvement over the traditional "3-term" random-walk models (i.e., a memory term, a random stochastic term, and one drift term accounting for the vertical gradient of σ_w) that have been successfully used in many air pollution studies, for urban applications the simplifying assumptions cited above are too constraining. For flows around buildings, there are strong mean winds and gradients of the mean wind and turbulence parameters in all three directions. In order to (partially) overcome the limitations of the equations cited above, we have implemented a local coordinate rotation scheme where the *x* direction is aligned with the mean wind vector and the *z* direction is aligned in the direction of the largest increase in the wind speed (a surrogate for the strongest gradient in turbulence).

This coordinate rotation is performed for each marker particle in the simulation using the mean wind vector at that particle location and the direction of the strongest wind shear at that location. Although the rotation scheme makes the equations messier (see Appendix A), it effectively allows for the model to account for non-zero $\overline{V}$ and $\overline{W}$ and horizontal gradients in the mean velocity and turbulence Reynolds stresses. It is only a partial solution with respect to gradients since we account for the gradient in the strongest direction only, not in all three directions simultaneously. One might ask why not just use the full set of equations as derived by Thomson (1987)? We decided against doing this because of the necessity of defining all the turbulence terms and the crudeness of the turbulence scheme that has been implemented into QUIC. That is, the additional fidelity of the equations with all their terms is offset by the lack of knowledge of the spatial variability of these turbulence terms.

b) Particle Reflection at Ground Surfaces, Walls, and Roofs

The approach to reflection is analogous to billiard ball type reflections as shown in Fig. 1. The reflection scheme needs to not only account for horizontal surfaces (the ground and rooftops), but vertical surfaces (walls) and the underside of horizontal surfaces (e.g., the bottom side of a bridge). The reflection algorithm is initiated when after moving a marker particle, it is found inside of a building or under the ground. The particle is then "reflected" as shown in Fig. 1 where its new position is equal to the distance "above" the reflecting surface (or to the right, to

the left, or below the reflecting surface depending on its orientation). Following Wilson and Flesch (1993), we reverse the sign of the velocity fluctuation component in the direction of the mean wind (not just the direction normal to the reflecting surface), i.e., $u_i'(t + \Delta t) = -u_i'(t)$ for i = 1, 2, and 3. This ensures that $\overline{u'w'}$ is of the right sign (i.e., negative) near the wall. Near the building base and the ground or where two buildings meet at right angles, we can also have the case where there is an "interior" corner with multiple reflections possible. For this case, we still utilize a billiard-ball reflection scheme. A maximum of two reflections is possible in one time step due to constraints on how far a marker particle can travel in one time step (see Section 3c). Note that there is no reflection of marker particles off the top of the domain; particles are allowed to exit the domain through the top at which point they are lost to the simulation.

c) Time Step Considerations

The size of the random-walk time step Δt is constrained by several conditions: it must be larger than the Kolmogorov time scale and smaller than the Lagrangian time scale so that the marker particle velocity is correlated over the time step Δt, while its acceleration is uncorrelated (e.g., Rodean, 1996). The Lagrangian time scale T_L, a measure of the correlation or persistence of turbulent eddies over time, becomes smaller near the surface, thus resulting in smaller time steps as the marker particle approaches the surface. According to Rodean (1996), the Lagrangian time scale can be estimated as:

$$T_L = \frac{2\sigma_w^2}{C_0 \varepsilon}.$$

An additional constraint is imposed that is similar to a Courant condition, i.e., the time step must be small enough so that a marker particle does not travel more than a (mean wind and turbulence field) grid cell during the time step. If this condition were not imposed, then the marker particle could travel over multiple grid cells and if the mean wind changes speed or direction over this distance or the turbulence intensity varies over this distance, then the particle would not "feel" the correct local wind and/or turbulence conditions during its flight. Internal to the QUIC-PLUME code, the Lagrangian time scale and Courant condition time step limits are computed and if violated, the code imposes smaller sub-time steps until the conditions are satisfied. Note

that time step constraints also operate on the dense gas spreading (slumping) velocity and the explosive rise buoyancy-induced vertical velocity (see Sections #.# and #.#, respectively, for more information).

d) Wind Interpolation to Particle Position

We estimate the mean wind components $\overline{U}$, $\overline{V}$, and $\overline{W}$ at the marker particle position (*x,y,z)* by using an inverse r^2-distance interpolation among the neighboring grid-cell center values. If the marker particle is within a half-grid cell of any surface (ground, wall, or roof), the velocity of the particle is estimated using a log-law extrapolation from the nearest grid cell using the wall roughness z_0.

e) Gravitational Settling

The gravitational settling velocity for an aerosol particle is based on Stokes' Law for the terminal velocity of spherical particles with a slip correction factor for small diameter (d_p) particles. The terminal velocity (v_s) is calculated using (e.g., Finlayson-Pitts, 1986; Seinfeld and Pandis, 1998):

$$v_s = \frac{1}{18}\frac{d_p^2 \rho_p g}{\mu_{air}} C_C,$$

where ρ_p is the particle density, g is gravitational acceleration, μ_{air} is the absolute viscosity of air, and C_C is the so-called Cunningham's correction factor. The correction factor is approximated by:

$$C_C = 1 + \frac{2\lambda}{d_p}\left[1.257 + 0.4\exp\left(-\frac{1.1 d_p}{2\lambda}\right)\right],$$

where λ is the mean free path of air. Seinfeld and Pandis (1998) show that the correction factor becomes more important for small particles, for example, C_C = 22.2, 2.85, 1.164, and 1.016 for d_p = 0.01, 0.1, 1 and 10 μm, respectively, at standard temperature and pressure.

The settling velocity is added directly to the mean vertical velocity computed by the wind solver (e.g., QUIC-URB, QUIC-CFD), such that:

$$z(t + \Delta t) = z(t) + (\overline{W} - v_s)\Delta t + w'(t)\Delta t$$

Note that the characteristic time scale to reach terminal velocity is very small, e.g., $3\text{x}10^{-4}$, $4\text{x}10^{-6}$, and $9\text{x}10^{-8}$ s for $d_p = 0.1$, 1 and 10 μm, respectively, so that use of the terminal velocity is a good approximation for the particle fall velocity.

f) Concentration Estimation

A user-defined 3D grid of sampling boxes is used to compute a concentration field. The tagged fluid parcels or aerosol particles representing the contaminant release are tracked at each random-walk time step Δt and the average concentrations are estimated by:

$$\overline{C}(x,y,z) = \sum_{time} \sum_{particles} \frac{m_p(1 - f_{decay}) \cdot (1 - f_{dep}) \cdot \Delta t}{Vol_{box} \cdot T_{avg}}$$

where the sum is over all marker particles that are found within the sampling box centered at location (x, y, z) and over the concentration averaging time T_{avg}. The mass represented by each marker particle m_p is normally specified at the beginning as n_{total}/Q (the total number of marker particles released during the simulation divided by the total mass released) and then is multiplied by the fractional terms 1-f_{decay} and 1-f_{dep} that account for mass loss over time through decay (e.g., UV decay) and surface deposition. For multi-particle size problems, the initial m_p for each particle can be particle-size dependent and based either on mass or number distribution. In addition, m_p itself can change with time for two-phase problems (see Section #.# on gas-liquid droplet capabilities) and for time-varying building exfiltration source terms. The volume of each sampling box $Vol_{box} = dx_b\, dy_b\, dz_b$, the length of the box in the x, y, and z directions, respectively. The code also computes the concentrations for particles smaller than a user-defined particle size, as well the dosage. As a post-processing step, the dosages can be converted into user-defined

thresholds, e.g., acute exposure guideline levels (AEGL's), lethal concentration thresholds (LCT's).

The statistical certainty of the computed average concentration $\overline{C}(x,y,z)$ is dependent on the number of particles released, the volume of the sampling box Vol_{box}, the averaging time T_{avg}, and the location of the sampling box relative to the source location. The statistical certainty is increased as more particles are released, as the sampling box is made bigger, and as the averaging time is made longer. Of course, the drawback is that the simulation takes longer for more particles, the spatial resolution of the computed concentration field is degraded for a larger sampling box, and the temporal resolution is degraded for a larger averaging time. Sampling boxes that are located along the plume centerline will result in many more marker particles traveling through these boxes, thus ensuring good statistical certainty in the computed average concentrations in this region. However, off the centerline, on the edges of the plume, fewer marker particles will travel there, so the statistical certainty will be lower in these regions. If one is interested in very low concentrations or dosages (e.g., a health effect threshold), then estimating the edges of the plume (i.e., the so-called "tails" of the plume) will become important and require either more particles to be released, a bigger sampling box, and/or a longer averaging time. An estimate of the minimum concentration that can possibly be calculated by the QUIC-PLUME model can be obtained by determining the concentration of a single particle in a sampling box for a single time step:

$$\overline{C}_{\min} = \frac{m_p \cdot \Delta t}{Vol_{box} \cdot T_{avg}} = \frac{Q \cdot \Delta t}{n_p \cdot Vol_{box} \cdot T_{avg}},$$

where the mass of one particle $m_p = Q/n_p$, Q is the total mass released and n_p is the total number of marker particles in the simulation. Here we have ignored the effects of deposition and decay and assumed that the release is either a gas or mono-disperse particles. A balancing act is required between the requirements placed on statistical certainty, simulation speed, spatial resolution, averaging time duration, and concentration minima.

g) Deposition Estimation

Deposition of gases and particles is computed internally in QUIC-PLUME if the deposition velocity scheme is turned on. We do not use a sticking factor approach, i.e., where some fraction of marker particles that impact surfaces stick to the surface and are then removed from the transport and dispersion simulation calculation. Rather, when marker particles are close to surfaces (within one grid cell) a fraction of the particle mass is lost to the surface using the traditional deposition velocity approach (e.g., Seinfeld and Pandis, 1998). In early versions of the code, the mass of material deposited was computed using:

$$M_{dep} = \sum_{particles} v_d \cdot \overline{C}_p \cdot A_{sfc} \cdot \Delta t,$$

where v_d is the deposition velocity (m/s), $\overline{C}_p$ is the concentration due to the particle in the grid cell, A_{sfc} is the surface area over which deposition is occurring (i.e., the surface area of the cell face that is touching the ground or a wall), Δt is the particle random-walk time step, and the summation is over all particles in the grid cell of interest. Using the random-walk time step Δt, we found that this approach worked well for small particles, but for large particles mass balance was compromised. For large particles, the random-walk time step Δt was too large, i.e., the gravitational settling velocity was large enough that a constant concentration assumption over a time step was invalid. The time step could have been made smaller to solve this problem, but this would significantly slow down the random-walk calculation.

In the current version of QUIC-PLUME, we still use the deposition velocity method, but instead we integrate the equations over the time step Δt in order to better estimate the mass flux for cases where Δt is large relative to the time scale of gravitational settling of the large particles. The equation is derived by first setting the rate of change of mass in the grid cell equal to the deposition rate:

$$\frac{dM_{cell}}{dt} = Dep_{rate} \Rightarrow V_{box} \frac{d\overline{C}_p}{dt} = v_d \cdot \overline{C}_p \cdot A_{sfc} \Rightarrow \frac{d\overline{C}_p}{dt} = \frac{v_d \cdot \overline{C}_p}{\Delta z_b} .$$

Note that if the deposition is occurring on vertical walls rather than a horizontal surface, Δz_b is replaced by Δx_b or Δy_b depending on the wall's orientation. We then integrate the differential equation over a time step Δt to obtain:

$$\frac{\overline{C}_p(t+\Delta t)}{\overline{C}_p(t)} = \exp\left(-\frac{v_d \cdot \Delta t}{\Delta z_b}\right).$$

The airborne concentration is reduced over the time step Δt exponentially due to deposition and is dependent on the magnitude of the deposition velocity v_d. The fraction of the marker particle mass lost to deposition is then just:

$$f_{dep} = 1 - \exp\left(-\frac{v_d \cdot \Delta t}{\Delta z_b}\right).$$

The mass deposited to the surface by the marker particle in one time step is:

$$M_{Dep} = m_p(t) \cdot \left\{1 - \exp\left(-\frac{v_d \cdot \Delta t}{\Delta z_b}\right)\right\}.$$

The total mass deposited is determined by summing over all particles in the collecting box of interest and summing over time. Deposition is reported cumulatively and is output at T_{avg} time intervals.

The deposition velocity v_d now needs to be determined. The user can either type in a value in the QUIC Graphical User Interface in the Source Term pop-up window (see Nelson et al., 2007) or the user can specify that the code internally computes the deposition velocity. The former option is usually done for gases, the latter option is usually done for aerosol particles. The method used by QUIC-PLUME for computing the deposition velocity is described below.

In the atmospheric chemistry community, it is standard practice to use a resistance-based approach to compute the deposition velocity (e.g., see Seinfeld and Pandis, 1998):

$$v_d = \frac{1}{r_a + r_b + r_a r_b v_s} + v_s$$

where r_a is the aerodynamic resistance, r_b is the quasi-laminar surface resistance, and v_s is the gravitational settling velocity. The calculation of the gravitational settling velocity is described above in Section 3e. Note that v_s is set to zero for vertical surfaces (e.g., walls) and for gases. Note also that the form of the equation above assumes that the surface or canopy resistance r_c = 0, a valid assumption for aerosol particles, but not for gases. Hence, this is why it is suggested to manually input a deposition velocity for gases rather than allowing the model to internally calculate the value.

The aerodynamic resistance r_a is the parameter that accounts for the impact of the turbulent atmosphere in transporting material from the air to a ground surface. In higher turbulence intensity environments dry deposition is enhanced, while for low turbulence intensities dry deposition is reduced. QUIC-PLUME uses the formula proposed by Sehmel and Hodgson (1978):

$$r_a = \frac{1}{\kappa u_*} \ln\left[\frac{\frac{10{,}000 u_* dz_b}{2\nu} + \frac{1}{Sc}}{\frac{100 u_*}{\nu} + \frac{1}{Sc}}\right],$$

where ν is the kinematic viscosity of air, $Sc = \nu/D$ is the Schmidt number, and D is mass diffusivity.

The quasi-laminar or surface resistance r_b represents the viscous layer(s) near surfaces through which the airborne contaminant must pass to get to the surface. For gases and small particles (St <10)

$$r_b = \frac{1}{u_* Sc^{-2/3}}$$

For large particles ($St > 10$)

$$r_b = \frac{1}{u_* \left(Sc^{-2/3} + 10^{-3/St} \right)}$$

where $St = v_s u_*^2 / g\nu$ is the Stokes number.

h) Decay

The decay scheme allows for each marker particle to lose mass (i.e., effectiveness, viability) with time due to environmental degradation or natural decay. The standard exponential decay equation is used:

$$f_{decay} = \exp\left[-\frac{t}{t_d} \right],$$

where t is the time since release of the marker particle and t_d is the decay time constant. The user specifies the value of t_d through the QUIC-GUI in the Source Term pop-up window (Nelson et al., 2007). Values can be found in the literature for biological agents, for example, as a function of relative humidity and the amount of sunshine.

4. Turbulence Parameterizations

The random-walk equations require knowledge of the Reynolds normal and shear stresses and the dissipation of turbulent kinetic energy. The QUIC wind solver computes the mean 3D wind field around buildings, but no information on turbulence. Including an Eulerian solver for a RANS k-epsilon turbulence scheme – like that found in many CFD codes – would defeat the purpose of the QUIC model: too run fast. Hence, we must make due with the mean wind field produced by the QUIC wind solver and develop a simple turbulence scheme. We have derived a scheme that uses both standard "local" (or gradient) mixing concepts combined with "non-local"

mixing algorithms. Additionally, we have made modifications to the definition of the turbulent length scale in the scheme for eddy vortices and for forest canopies and to account for stratification (stability) effects. We will describe these turbulence parameterizations below.

a) Turbulence Similarity Relationships

In the surface (constant stress) layer, dimensional analysis combined with experiments have resulted in well-known relationships between the friction velocity u_*, the Monin-Obukhov length L, and turbulence parameters, i.e., Monin-Obukhov surface layer similarity parameterizations (e.g., Arya, 1988). Although these relationships may not hold exactly around buildings where the flow field is significantly more complex, by necessity we utilize these relationships to determine the turbulence parameters needed in the random-walk equations described above (note that Hanna (2007) has shown that the relationships hold approximately based on their analysis of recent turbulence measurements in cities). We also must compute turbulence parameters above the surface layer and thus use corrections based on the distance above the ground normalized by the boundary-layer height following the approach provided in Rodean (1996).

The relationships used in QUIC for neutral through stable conditions ($z/L \geq 0$) are:

$$\sigma_u^2 = 6.25 u_*^2 \left(1 - \frac{z}{h}\right)^{3/2},$$

$$\sigma_v^2 = 4 u_*^2 \left(1 - \frac{z}{h}\right)^{3/2},$$

$$\sigma_w^2 = 1.96 u_*^2 \left(1 - \frac{z}{h}\right)^{3/2},$$

$$\tau_{13} = -u_*^2 \left(1 - \frac{z}{h}\right)^{3/2}, \text{ and}$$

$$\varepsilon = \frac{u_*^3}{k(d_{wall} + z_0)} \left(1 + 3.7 \frac{z}{L}\right) \left(1 - 0.85 \frac{z}{h}\right)^{3/2}.$$

where k is the von Karman constant (chosen as 0.4), d_{wall} is the shortest distance to a surface (e.g., the ground surface, a wall, a rooftop, the underside of an obstacle), z_0 is the wall roughness length, and h is the boundary-layer depth.

For unstable conditions ($z/L < 0$), the relationships are:

$$\sigma_u^2 = 6.25u_*^2\left(1-\frac{z}{h}\right)^{3/2} + 0.6u_*^2\left(-\frac{h}{L}\right)^{2/3}$$

$$\sigma_v^2 = 4.5u_*^2\left(1-\frac{z}{h}\right)^{3/2} + 0.6u_*^2\left(-\frac{h}{L}\right)^{2/3}$$

$$\sigma_w^2 = 1.69u_*^2\left(1-\frac{z}{h}\right)^{3/2} + 3.3u_*^2\left(-\frac{z}{L}\right)^{2/3}\left(1-0.8\frac{z}{h}\right)^2$$

$$\tau_{13} = -u_*^2\left(1-\frac{z}{h}\right)^{3/2+\frac{h/L}{2(1-h/L)}}, \text{ and}$$

$$\varepsilon = \frac{u_*^3}{k(d_{wall}+z_0)}\left(1-0.75\frac{z}{L}\right)\left(1-0.85\frac{z}{h}\right)^{3/2} + 0.3\frac{z}{L}.$$

The entire suite of turbulence parameters can be obtained with knowledge of the friction velocity u_*, the Monin-Obukhov length L, and the boundary layer height h. The latter two variables are input parameters to QUIC, while the friction velocity is computed internally using both local (i.e., gradient or K-theory) and non-local turbulence schemes.

b) Local (Gradient) Mixing Scheme

The scaling velocity for turbulence in the surface layer, i.e., the friction velocity, is defined as the square-root of the absolute value of the Reynold's shear stress at or near the surface. Around buildings, where turbulence is highly inhomogeneous, a single turbulent scaling velocity is not possible. Instead we define a "spatially-varying" friction velocity, i.e., a u_* that varies with location x, y, and z and that is equated to the square root of the absolute value of the spatially-

varying Reynolds shear stress (with some corrections for height dependence and stability as shown immediately above in the equation for τ_{13}).

The key then is how to specify a spatially-varying $u_*(x,y,z)$ so that all the turbulence parameters defined in Section 4a can be computed. QUIC-PLUME uses two approaches: one that is based on a local gradient turbulence closure, the other described in the next section that is based on a non-local closure scheme. Note that the gradient scheme is called a "local" scheme because u_* at a point (x,y,z) is equated to other variables at that same location (x,y,z). A "non-local" scheme implies that $u_*(x,y,z)$ will be specified using variables at locations at a distance from the location (x,y,z).

The gradient-based scheme specifies the spatially-varying friction velocity using simple mixing length arguments (e.g., Pasquill, 1974):

$$u_{*L}(x,y,z) = \frac{k \cdot d_{wall}}{\phi_m} \left. \frac{\partial V_{mag}}{\partial r} \right|_{\max},$$

where k is von Karman's constant, d_{wall} is the shortest distance to a surface, V_{mag} is the velocity magnitude (or equivalently total wind speed), r is the direction perpendicular to the mean velocity vector that provides the largest gradient in velocity magnitude, and ϕ_m an atmospheric stability correction term that is computed via Pielke (1984):

$$\phi_m = 1 + 4.7\frac{z}{L} \qquad \text{for } z/L \geq 0, \text{ and}$$

$$\phi_m = \left(1 - 15\frac{z}{L}\right)^{-1/4} \qquad \text{for } \frac{z}{L} < 0.$$

Within a grid cell of a surface where there are not sufficient points to estimate the total velocity gradient, we obtain $u_{*L}(x,y,z)$ by assuming a log-law profile near the surface:

$$u_{*L}(x,y,z) = \frac{kV_{mag}(x,y,z)}{\ln\left(\frac{d_{wall}}{z_0}\right) - \varphi_m\left(\frac{z}{L}\right)},$$

where φ_m is given by:

$$\varphi_m(z/L) = -4.7z/L \qquad \text{for } \frac{z}{L} \geq 0 \text{ and}$$

$$\varphi_m(z/L) = 2\left[\ln\left(1+\phi_m^{-1}\right)/2\right] + \ln\left[\left(1+\phi_m^{-2}\right)/2\right] - 2\tan^{-1}\phi_m^{-1} + \pi/2, \qquad \text{for } \frac{z}{L} < 0.$$

Where there are flow reversals, i.e., standing eddies, or strong shear far from a wall, we want to compute a turbulent length scale that is measured from the center of the eddy or between the two zones where the shear is created, rather than the distance to the wall. In locations at least two grid cells from the wall, we take the minimum of

$$l_{mix} = kV_{mag} / \left|\partial V_{mag} / \partial r\right| \quad \text{and} \quad l_{mix} = k \cdot d_{wall}$$

to plug into the equation for u_{*L}. Note that u_{*L} is not allowed to go below 0.03 m/s.

It is important to point out that we have assumed that the large amount of mechanical mixing close to the buildings results in neutral stability. Hence, in regions where building flow parameterizations are applied, the Monin-Obukhov length L is set to infinity. Stability effects on the turbulence parameters are still felt above the buildings and between widely-spaced buildings.

Within QUIC-PLUME, the turbulence parameters are computed in the local rotated coordinate system. For example, σ_u refers to the standard deviation in the direction of the mean wind vector. We feel that this more closely follows the spirit of the original surface layer similarity theory where although developed for horizontally homogeneous flow over flat terrain, the σ's were derived with an implicit alignment to the prevailing wind. One problem that develops in implementing such a scheme is that if the mean winds change rapidly with distance the local coordinate system also changes orientation at each time step as the marker particle travels. To

overcome the problem of referencing a random velocity fluctuation from one time step to the next in the likely case of the local coordinate system having changed, QUIC-PLUME converts the random velocities from the prior step to the fixed coordinate system and then rotates the velocity fluctuation components into the new local coordinate system before the random-walk equations for du', dv', and dw' are invoked. The translation equations between the fixed and local coordinate systems are given in Appendix B.

c) Non-Local Mixing Scheme

Wind-tunnel experiments, full field observations, and large-eddy simulation of flow around buildings exhibit eddies that sweep contaminants across, into, or out of the cavities and recirculation zones around buildings. The measured concentrations suggest that there is considerable mixing in the wakes of buildings and that material is physically-transported across relatively large distances by intermittent large eddies, i.e., non-local mixing is an important component of transport and dispersion around buildings.

Mixing by large eddies is, for example, an important process in the daytime convective boundary layer and gradient-based turbulence schemes have been shown to fail for these cases (e.g., Stull, 1989; Pleim and Chang, 1992). Sreenivasen et al. (1982) wrote that "there is general awareness that in turbulent shear flows, transport occurs not only by the diffusive motion of the small eddies (as envisaged by the gradient transport models) but also by the motion of large eddies comparable in size to the flow width." Townsend (1956) was one of the first to add a non-local mixing term to a turbulence closure scheme. Based on similar ideas, Blackadar (1978) developed a non-local mixing scheme for the convective boundary layer that is used in the MM5 mesoscale meteorological code.

For flows around buildings, the non-local mixing process was conceptualized as driven by velocity differences between the winds passing by the sides or over the tops of buildings and the lighter winds in the downwind cavity, between buildings in the street canyon, or in other recirculation zones. That is, periodically, large gusts of high momentum air are ingested into the building recirculation zones by large eddy mixing processes. Two situations were considered: mixing produced by vertical-axis (horizontally-rotating) eddies that transport fluid horizontally

and mixing produced by horizontal-axis (vertically-rotating) eddies that bring fast moving air down from above.

In the case of horizontal mixing, the non-local mixing length scale l_{NL} is chosen as the half-width of the downwind cavity (which is identical to the building half-width for flow perpendicular to the building, but greater than the building half-width for oblique angle flow) and the velocity difference was calculated by taking the difference of the mean winds at the edge of the building with those along the centerline of the cavity:

$$\Delta u_{ref}(d,z) = s_{w/2^+}(-\frac{l}{2},z) - s_a(d,z)$$

where $s_{w/2^+}$ is the wind speed just outside the building at its center in the lengthwise direction and $s_a(d,z)$ is the speed on the axis of the wake or cavity at a distance d from the nearest wall of the building. Horizontal non-local mixing is assumed to produce a non-local friction velocity of:

$$u_{*NL-H}(x,y,z) = k\Delta u_{ref}(d,z),$$

for all points inside the wake or cavity that satisfy:

$$s(d,y,z) \le .8 * \Delta u_{ref}(d,z),$$

with y measured transverse to the downwind axis of the building. The effective width of the building and the length of the wake or eddy provide the region for which non-local mixing is considered. The parameters describing the wake or eddy are provided by QUIC-URB output as:

$$d_w = 3l_r$$

with d_w the distance from the back wall of the building to the end of the wake, and L_{fx} the distance in the x-direction to the upstream limit of the front eddy, and L_{fy} the distance in the y-direction to the upstream limit of the cavity. Figure 4 illustrates the geometry
The coordinate system relevant to horizontal mixing is assumed to be aligned with the mean wind. In the coordinate system aligned with the mean wind we use:

$$\overline{u_{gf}^2} = 4u_{*g}^2,$$

$$\overline{w_{gf}^2} = 4u_{*g}^2,$$

and

$$\overline{v_{gf}^2} = 1.69u_{*g}^2.$$

For the shear stresses we use:

$$\overline{u_{gf}v_{gf}} = -\frac{y - y_a}{y_{w/2+}}u_{*g}^2$$

and

$$\overline{u_{gf}w_{gf}} = \overline{v_{gf}w_{gf}} = 0.$$

For mixing in the vertical direction (eddies whose axis is horizontal), the reference wind speed is that directly above the point of interest and it is compared to a zero speed at the ground or rooftop. We describe the friction velocity as:

$$u_{*gz}(d,y) = s_{ht+}(d,y)$$

with $s_{ht+}(d,y)$, the mean speed at the height of the building top plus one cell at a distance d from the building wall and a transverse distance y. The relevant stresses are:

$$\overline{u_{gf}^2} = 4u_{*gz}^2,$$

$$\overline{v_{gf}^2} = 4u_{*gz}^2,$$

$$\overline{w_{gf}^2} = 1.69u_{*gz}^2,$$

$$\overline{u_{gf}w_{gf}} = -u_{*gz}^2,$$

and,

$$\overline{u_{gf}v_{gf}} = \overline{v_{gf}w_{gf}} = 0.$$

The choice between horizontal mixing and vertical mixing is made based on the largest average gradient of the mean wind. Specifically if:

$$\frac{\Delta u_{ref}(d,z)}{w_{teff}/2} \geq \frac{s(d,y,z)}{ht_{eff}},$$

the mixing is dominated by the horizontal mixing. Otherwise, vertical mixing is assumed. The same point in the wake or eddy may be influenced by more than one building and we choose the building that has the largest u_{*g}.

d) Modifications to Turbulence Scheme for Forest (and Urban) Canopies

The QUIC wind solver has drag parameterizations for forest (and urban) canopies that act to slow the wind down (Nelson et al, 2009). Trees are not explicitly resolved, rather the model accounts for their bulk effect of wind speed reduction. This wind flow parameterization results in fairly strong velocity gradients at the top of the forest canopy (and to a lesser extent at the sides of the canopy). In early versions of QUIC-PLUME, unrealistically large u_* values were computed above the canopy top mostly due to incorrectly specifying the mixing length as the distance from the ground surface, rather than the canopy top.

We have developed adjustments for turbulence in the presence of vegetative canopies by changing the turbulence length scale within and above the top of the canopy. The canopy length scale is based on MacDonald (2000):

$$l_{canopy} = \alpha^{-1} \frac{u_*}{U_H} H_{canopy},$$

where α is the canopy attenuation coefficient (e.g., see Cionco, 1972), u_* is the friction velocity derived from the ambient velocity profile, U_H is the wind speed at canopy top, and H_{canopy} is the height of the canopy.

We divide the canopy into three zones. From the surface to 3/10 of the canopy height, the mixing length is assumed to increase linearly with height (Pardyjak et al., 2008):

$$l_{mix} = l_{canopy} \frac{z}{0.3H_{canopy}}$$

where z is measured from the top of the domain roughness length z_0. From 3/10 H_{canopy} to just below the canopy top, the eddy mixing length is assumed to be constant:

$$l_{mix} = l_{canopy}.$$

Finally, near the canopy top, a vortex algorithm (see Section 4b) is used to find the mixing length in the high shear flow zone at the last cell within the canopy:

$$l_{mix} = \kappa V_{mag} \left(\frac{dV_{mag}}{dz} \right)^{-1}.$$

Above the canopy, the smaller of the mixing lengths computed using the vortex algorithm above or the height dependent algorithm below is used:

$$l_{mix} = \kappa (z - H_{canopy}) + l_{canopy}.$$

Note that Nelson et al (2009) have found reasonable agreement in the computed turbulence using this scheme when compared to wind-tunnel canopy experiments performed by Finnigan and Mulhearn (1978).

e) Modifications to Turbulence inside the Dense Gas Cloud

Measurements of turbulence within dense gas clouds have shown that turbulence is damped relative to the surrounding atmosphere (e.g., Briggs et al., 2001). In the QUIC-PLUME turbulence scheme, the friction velocity u_* computed using the methods shown above is reduced inside the dense gas cloud following Briggs et al. (2001):

$$u_{*dg} = \frac{u_*}{1 + 0.2Ri_b},$$

where u_{*dg} is the friction velocity inside the dense gas cloud and Ri_b is the bulk Richardson number. The bulk Richardson number is defined as:

$$Ri_b = gh\frac{\rho_{dg} - \rho_{air}}{\rho_{air}u_*^2},$$

where g is gravitational acceleration, h is the dense gas cloud depth, ρ_{dg} is the dense gas cloud density, and ρ_{air} is the air density. The bulk Richardson number changes with time as the dense gas cloud slumps (h decreases) and then entrains fresh air (ρ_{dg} decreases and h eventually increases). More information on the dense gas cloud algorithms is found in Section 8.

f) Modifications to Turbulence inside the RDD Explosive Release

Measurements of turbulence within dense gas clouds have shown that turbulence is damped relative to the surrounding atmosphere (e.g., Briggs et al., 2001). In the

5. Source Geometries

QUIC-PLUME has several different starting geometries for specifying the source distribution. For most release types, the airborne contaminant can be released from a spherical volume, a spherical shell, a rectangular volume, a cylindrical volume, a line, or a moving point source.

Area sources can be approximated by thin rectangular or cylindrical volumes. Point sources can be approximated by a small diameter spherical volume source. Line and moving point sources can be constructed out of multiple line segments. For the moving point source a beginning velocity and ending velocity is specified for each line segment. If the begin and end velocities are different, the velocity is linearly interpolated over the segment length.

For many release types, multiple sources can be specified, e.g., a rectangular volume source in one part of the domain, a line source in another, and two spherical volume sources in another. If multiple sources are specified, the user must specify the amount of mass released for each source. In addition, the user specifies the total number of marker particles to be released during the simulation. An important point to understand is that the QUIC-PLUME code needs to divvy up the total number of marker particles and associate them with each source. Currently, the QUIC-PLUME code divides up the particles weighted by the release mass of each source, i.e., if 100,000 marker particles were specified for a for a two-source problem where 100 grams is released from one source and 25 grams from a second source, then 80,000 particles would be released from the first source and 20,000 from the second source. For the volumetric and line sources, the Lagrangian marker particles are released uniformly over the source region. For the moving point source, the marker particles are released at a constant rate per unit time.

Currently, dense gases can only be specified as ground-level cylindrical releases and radiological dispersal devices (RDD's) as hemispherical ground-level releases. Multiple sources can be specified for dense gases, but not for RDD's. Most source types can be specified as instantaneous, finite duration, or continuous releases. The exceptions are dense gases (instantaneous or continuous only) and RDD's (instantaneous only).

A relatively new capability is the exfiltration source type. If the building infiltration scheme is turned on (see Section #), the exfiltration source type can be used to account for the airborne contaminant that is mechanically or naturally ventilated out of a building. More information on building exfiltration can be found in Section #.

6. Multi-Particle Size Capability

In addition to stipulating a single particle size for a release, the user can prescribe log normal size distributions or histograms using multiple size bins. For multiple size bin problems, the user defines the mass fraction in each size bin and the particle diameter is set to the center of the size bin (e.g., the particle diameter is set to 7.5 microns for the 5-10 micron bin). Alternatively, the particle size distribution can be described in a continuous fashion using log-normal functions for mass or particle number distributions:

$$f(D_p) = \frac{1}{\sqrt{2\pi} D_p \ln\sigma_g} \exp\left(\frac{\left(\ln D_p - \ln \overline{D}_p\right)^2}{2\ln^2 \sigma_g} \right),$$

where D_p is the particle diameter, $\overline{D}_p$ is the mass median diameter (MMD) or the count median diameter (CMD), and σ_g is the geometric standard deviation. If multiple log-normal distributions are used, the mass or particle number fraction for each log normal also needs to be given. Note that the GUI allows the user to specify the distributions by mass- or particle number and can convert between the two using (e.g., Pandis and Seinfeld, 1998):

$$\ln \overline{D}_p(MMD) = \ln \overline{D}_p(CMD) + 3\ln^2 \sigma_g$$

Each marker particle in the simulation is given a particle diameter based on the particle size distribution. For problems with aerosol particle distributions defined by size bins, the number of marker particles put into each size bin is directly proportional to the mass fraction of each size bin. For continuous distributions, the number of marker particles that are given a specific diameter is weighted by either the mass or number distribution. If the number distribution option is selected, that means more marker particles will be in the small diameter sizes as compared to using a mass distribution. The option to specify is in part determined by the size range that is most important to the problem and the natural distribution of particles. For example, if a release has a lot of mass in the 200 microns and greater particle size range and the user is interested in the <10 micron breathable fraction, specifying by count fraction could provide more statistically-certain mean concentrations for the breathable fraction.

7. Bio-Slurry Source

The user can select a bio-slurry source in which biological agent (or any non-soluble material) is suspended in a water solution and emitted as a droplet spray. The user specifies the amount of agent, the initial droplet size distribution, the concentration of solids in the solution (includes the bio agent itself plus other inert solids), the effective density of the dry agglomerate, the relative humidity and temperature of the air, and the atmospheric pressure. The droplets will evaporate with time as they move through the air while simultaneously being pulled downwards by gravity. When the water content is completely evaporated, a dry particle made up of biological agent and inert solids will be tracked. The size of the dry particle is determined by the initial concentration of solids in the solution and by the effective density of the dry agglomerate. The former determines the solids mass in each droplet and the latter provides an estimate of how tightly packed the biological agent (e.g., spores, cells) and inert solids are when dry.

The evaporation algorithm is enacted for marker particles (i.e., water droplets) that have a radius that is larger than the minimum radius (equal to the dry agglomerate particle radius). The time rate of change of the droplet radius r [m] due to evaporation is computed using:

$$\frac{dr}{dt} = \frac{D_{corr}\left(101325(P_v - P_d)\right)}{(1\times 10^6\rho)r\left(\frac{D_{corr}H_v(101325P_d)\left(\frac{H_v}{RT}-1\right)}{M_v k_{corr} T} + \frac{RT}{M_v}\right)}$$

where dr/dt is the time rate of change of the droplet radius [m/s], D_{corr} is the corrected diffusion coefficient of water vapor in air [m^2/s], P_v is the ambient water vapor pressure of the atmosphere [atm], P_d is the vapor pressure of water at the surface of the droplet [atm] (the factor of 101,325 converts both vapor pressures into Pascals), ρ is the density of liquid water [g/mL] (the factor of $1x10^6$ converts the density to g/m^3), H_v is the heat of vaporization of water [J/mol], R is the universal gas constant [8.314151 J/(molK)], T is the local atmospheric temperature [K], M_v is the molecular weight of water agent vapor [g/mol] and k_{corr} is the corrected thermal conductivity of air [W/(mK)]. Below we show how each of these terms is computed.

To obtain D_{corr}, the molecular diffusion coefficient D [m^2/s] is first computed based on Hall and Pruppacher (1976) and Pruppacher and Klett (1978):

$$D = 2.11 \times 10^{-5} \left(\frac{T}{T_0}\right)^{1.94} \left(\frac{P_0}{P}\right)$$

where T_0 is the reference air temperature [273.15 K], P_0 is the reference pressure [1 atm], T is the local air temperature [K], and P is the local pressure [atm]. The diffusion coefficient is then corrected for non-continuum effects through ventilation and collision geometry terms:

$$D_{corr} = D\frac{C_{vent}}{C_{coll}}.$$

The ventilation coefficient C_{vent} is a function of the Reynolds number ($Re = Ud/\nu$) and the Schmidt number ($Sc = \nu/D$), where U is the droplet speed [m/s], d is the particle diameter [m], and ν is the kinematic viscosity of air [m^2/s]:

$$C_{vent} = 1 + 0.108\,\mathrm{Re}\,Sc^{2/3} \qquad \text{for } \mathrm{Re}^{1/2}Sc^{1/3} \le 1.4$$
$$C_{vent} = 0.78 + 0.308\,\mathrm{Re}^{1/2}\,Sc^{1/3} \qquad \text{for } \mathrm{Re}^{1/2}Sc^{1/3} > 1.4.$$

The collision coefficient C_{coll} is a function of a geometry coefficient and a sticking coefficient:

$$C_{coll} = 1 + (C_{geom} + C_{stick})\frac{MFP}{r}$$

where

$$C_{geom} = 1.33 + \frac{0.70r/MFP}{1 + r/MFP} \text{ and}$$

$$C_{stick} = \frac{4 \cdot (1 - E_{stick})}{3E_{stick}}.$$

Here, r is the radius of the droplet [m], MFP is the mean free path of water in the vapor phase [m], and E_{stick} is the sticking efficiency [0-1]. For water vapor, the sticking efficiency is set to one.

The vapor pressure P_v of the ambient atmosphere is determined from the relative humidity profile and the saturation vapor pressure of water:

$$P_v(z) = rh(z) * P_{sat} .$$

The saturation vapor pressure P_{sat} [atm] is computed using:

$$P_{sat} = P_{sat0} exp\left(\frac{M_v}{R}\left(A\left(\frac{T - T_0}{T T_0}\right) + B ln\left(\frac{T}{T_0}\right)\right)\right)$$

where P_{sat0} is the reference vapor pressure of water [6.03 X 10^{-3} atm], M_v is the molecular weight of water vapor [g/mol], R is the universal gas constant [8.314151 J/(molK)], T is the atmospheric temperature as function of height [K], T_0 is the reference temperature [273.15 K], A has a value of 3.14839 X 10^3 J/g, and B has a value of 2.370 J/(gK).

The vapor pressure of water at the surface of the droplet P_d [atm] is

$$P_d = P_{sat} \exp\left[\frac{2\sigma M_{liq}}{rRT(1x10^6 \rho_{liq})}\right],$$

where σ is the surface tension of the water droplet [N/m], M_{liq} is the molecular weight of liquid agent [g/mol], r is the radius of the droplet [m], and ρ_{liq} is the liquid density of the agent [g/mL] (the factor of 1X10^6 converts the density to g/m^3). The water droplet surface tension is calculated using:

.

$$\sigma = 0.001 \cdot (76.1 - 1.55(T - T_0)) \quad \text{if T} \geq \text{T}_0$$

$$\sigma = \sum_{i=1}^{7} \alpha_i (T - T_0)^i \quad \text{if T} < \text{T}_0$$

where $\alpha_1 = 7.593 \times 10^{-2}$, $\alpha_2 = 1.15 \times 10^{-4}$, $\alpha_3 = 6.818 \times 10^{-5}$, $\alpha_4 = 6.511 \times 10^{-6}$, $\alpha_5 = 2.933 \times 10^{-7}$, $\alpha_6 = 6.283 \times 10^{-9}$, and $\alpha_7 = 5.285 \times 10^{-11}$.

The heat of vaporization H_v [J/mol] is determined from

$$H_v = (2501 - 2.37 \cdot (T - T_0)) \cdot M_{liq},$$

while the corrected thermal conductivity of air k_{corr} [W/(mK)] is specified using:

$$k_{corr} = k \frac{C_{vent}}{C_{coll}},$$

where C_{vent} and C_{coll} are as defined above with the exception of the Schmidt number, the mean free path of the agent vapor, and the sticking efficiency being replaced with the Prandtl number ($Pr = \rho \nu C_p / k$, where C_p is the heat capacity of air [J/(kgK)]), the mean free path of air, and the thermal accommodation of air [units?], respectively.

8. Dense Gas Model

a) Instantaneous Release.

The dense gas model uses a combination slab and random-walk modeling approach. The slab model (e.g., Hanna and Drivas, 1987) is used to define the outflow and slump velocities of the random-walk marker particles and is used to define the region of reduced turbulence (as described in Section 4e). That is, a marker particle at *(x, y, z)* within the dense gas slab is moved with the mean velocity Ui(x,y,z) produced by the QUIC-URB wind solver, the turbulent

fluctuating velocity ui'(x,y,z,t) computed by the QUIC-PLUME random-walk equations, and the outflow velocity Vdg and the vertical slump velocity dh/dt calculated by the slab model.

the can leave the slab through turbulence and mean motions

7. Radiological Dispersal Device Capability

Indoor Capability (Werley's ppt)

Exfiltration (matt?)

Two-Phase Flow

$$P_v(i,j,k) = \sum_{n=1}^{N} \frac{m_n RT(i,j,k)}{101325 MV}$$

where m_n is the mass of agent vapor in cell (i,j,k) [g], T is the temperature in cell (i,j,k) [K], M is the molecular weight of water [g/mol], V is the volume of the cell (i.e., dx*dy*dz) [m^3], and the constant 101, 325 converts the vapor pressure from Pascals to atmospheres.

References

Allwine, K.J., J.E. Flaherty, M. Brown, W. Coirier, O. Hansen, A. Huber, M. Leach, and G. Patnaik, 2008: Urban Dispersion Program: Evaluation of six building-resolved urban dispersion models, Official Use Only PNNL-17321 report, 88 pp.

Anfossi, D., F. Desiato, G. Tinarelli, G. Brusasca, E. Ferrero, and D. Sachhetti, 1998: TRANSALP 1989 Experimental Campaign: II. Simulation of a tracer experiment with Lagrangian particle models, *Atmospheric Environment* **32**: 1157-1166.

Antoine, C., 1888: Tensions des Vapeurs: Nouvelle Relation Entre les Tensions et les Températures, *Compt. Rend.*, **107**, 681.

Arya, S. P. S., 1988: Introduction to Micrometeorology. Academic Press, New York, NY, 320 pp.

Blackadar, A. K., 1978: Modeling pollutant transfer during daytime convection. AMS Fourth Symp. on Atmospheric Turbulence, Diffusion, and Air Quality, Reno, NV, 443–447.

Bowker, G., R. Baldauf, V. Isakov, A. Khlystov, and W. Petersen, 2007a: The effects of roadside structures on the transport and dispersion of ultrafine particles from highways, *Atmospheric Environment* **41**: 8128-8139.

Bowker, G., D. Gillette, G. Bergametti, B. Marticorena, and D. Heist, 2007b: Sand flux simulations at a small scale over a heterogeneous mesquite area of the northern Chihuahuan desert, *Journal of Applied Meteorology* **46**: 1410-1422.

Bowker, G., S. Perry, and D. Heist, 2004: A comparison of airflow patterns from the QUIC model and an atmospheric wind tunnel for a two-dimensional building array and multi-block region near the World Trade Center site, 5th AMS Urban Env. Conf., Vancouver, B.C., 6 pp.

Brown, M., A. Gowardhan, M. Nelson, M. Williams, E. Pardyjak, 2009: Evaluation of the QUIC wind and dispersion models using the Joint Urban 2003 Field Experiment, AMS 8th Symp. Urban Env., Phoenix, AZ.

Cionco, R., 1972: A wind-profile index for canopy flow, *Boundayer-Layer Meteorology* **3**: 255-263.

Eötvös, R., 1886: Ueber den Zusammenhang der Oberflächenspannung der Flüssigkeiten mit ihrem Molecularvolumen, *Ann. der Physik*. **263**: 448-459.

Favaloro, T., E.R. Pardyjak, M. Brown, 2007: Toward understanding the sensitivity of the QUIC dispersion modeling system to real input data, AMS 7th Symp. Urban Env., San Diego, CA, paper 10.3, 10 pp.

Finnigan, J. J. and P. J. Mulhearn, 1978: Modeling waving crops in a wind tunnel. *Boundary-*

Layer Meteorology **14**: 253-277.

Fuller, E.N., P.D. Schettler, and J.C. Giddings, 1966: A New Method for Prediction of Binary Gas-Phase Diffusion Coefficients, *Ind. Eng. Chem.* **58**: 19-27.

Gowardhan, A., M. Brown, E.R. Pardyjak, 2007: Evaluation of a fast response pressure solver for flow around an isolated cube, *Journal of Environmental Fluid Mechanics,* submitted, LA-UR-07-4016.

Gowardhan, A., M. Brown, M. Williams, E. Pardyjak, 2006: Evaluation of the QUIC Urban Dispersion Model using the Salt Lake City URBAN 2000 Tracer Experiment Data- IOP 10. 6th AMS Symp. Urban Env., Atlanta, GA, LA-UR-05-9017, 13 pp.

Hanna, S., J. White, Y. Zhou, 2007: Observed winds, turbulence, and dispersion in built-up downtown areas of Oklahoma City and Manhattan, *Boundary-Layer Meteorology* **125**: 441-468.

Hurley, P.J., Physick, W.L., Luhar, A.K., 2005. TAPM: a practical approach to prognostic meteorological and air pollution modelling. *Environmental Modelling and Software* **20**: 737-752.

Klein, V.A., 1949: Latent Heats of Vaporization, *Chem. Eng. Prog.*, **45**, 675.

Ley, A. 1982: A random-walk simulation of two-dimensional turbulent diffusion in the neutral surface layer, *Atmospheric Environment* **16**: 2799-2808.

Lyman, W.J., W.F. Reehl, and D. H. Rosenblatt, 1982: *Handbook of Chemical Property Estimation Methods*, McGraw-Hill, New York, USA.

MacDonald, R. W., 2000: Modeling the Mean Velocity Profile in the Urban Canopy Layer, *Boundary-Layer Meteorology* **97**: 25-45.

Nelson, M., B. Addepalli, D. Boswell, and M. Brown, 2007: QUIC Start Guide (v. 4.4), LA-UR-07-2799, 123 pp.

Nelson, M.A., M. D. Williams, D. Zajic, E. R. Pardyjak, and M. J. Brown, 2009: Evaluation of an Urban Vegetative Canopy Scheme and Impact on Plume Dispersion, AMS 8th Symp. Urban Env., Phoenix AZ, LA-UR-09-00068.

Pardyjak, Eric R. and Michael J. Brown, 2001, Evaluation of a Fast-Response Urban Wind Model – Comparison to Single-Building Wind Tunnel Data, LA-UR-01-4028, Los Alamos National Laboratory.

Pardyjak, E.R. and M. Brown, 2003: QUIC-URB v. 1.1: Theory and User's Guide, LA-UR-07-3181, 22 pp.

Pasquill, F., 1974: Atmospheric Diffusion, A Study of the Dispersion of Windbourne Material from Industrial and Other Sources, Ellis Horwood Limited.

Pielke, R. A., 1984: Mesoscale Meteorological Modeling, Academic Press.

Pleim, J.E. and J. S. Chang, 1992: A non-local closure model for vertical mixing in the convective boundary layer, *Atmospheric Environment* **26A**: 965–981.

Pruppacher, H.R. and J.D. Klett, 1978: Microphysics of Clouds and Precipitation, D. Reidel Publishing Co., Dordrecht, Holland.

Röckle, R., 1990: Bestimmung der stomungsver-haltnisse im Bereich Komplexer Bebauugsstruk-turen. Ph.D. thesis, Vom Fachbereich Mechanik, der Technischen Hochschule Darmstadt, Germany.

Rodean, H. C., 1996: Stochastic Lagrangian Models of Turbulent Diffusion, The American Meteorological Society, 82 pp.

Sehmel G. and W. Hodgson, 1978: A model for predicting dry deposition of particles and gases to environmental surfaces, Report PNL-SA-6721, 51 pp.

Seinfeld, J.H. and S.N. Pandis, 1998: Atmospheric Chemisty and Physics: From Air Pollution to Climate Change. Wiley Interscience, New York, NY, 1326 pp.

Senocak, I., A. Gowardhan, and M. Brown, 2007: Evaluation of the QUIC Fast Response Dispersion Modeling System with the New York City Madison Square Garden (MSG05) Field Study: IOP 1, Release 2, draft, 55 pp.

Singh, B., B. Hansen, M. Brown, E. Pardyjak, 2008: Evaluation of the QUIC-URB fast response urban wind model for a cubical building array and wide building street canyon, *Environmental Fluid Mechanics* **8**: 281-312.

Sreenivasan, K., S. Tavoularis, S. Corrsin, 1982: A test of gradient transport theory and its generalizations, Turbulent Shear Flows 3: Third International Symposium on Turbulent Shear Flows, Davis, CA, USA

Stull, R., 1989: An Introduction to Boundary Layer Meteorology, Kluwer Academic Press, Boston, MA, 666 pp.

Thomson, D.J., 1987: Criteria for the selection of stochastic models of particle trajectories in turbulent flows, *Journal Fluid Mechanics* **180**: 529-556.

Townsend, A.A., 1956: The Structure of Turbulent Shear Flow, Cambridge University Press, Cambridge, UK, 315 pp.

Weil, J., 2005: Comments on QUIC-PLUME Theory Guide (Williams et al., 2004), 4 pp, internal report.

Williams, M. and M. Brown, 2004: QUIC-PLUME Advanced User's Guide, LA-UR-04-0562, 21 pp.

Williams, M., M. Brown, D. Boswell, B. Singh, and E. Pardyjak, 2004: Testing of the QUIC-PLUME model with wind-tunnel measurements for a high-rise building, 5th AMS Urban Env. Conf., Vancouver, B.C., LA-UR-04-4296, 10 pp.

Wilson, J.D. and T.K. Flesch, 1993: Flow boundaries in random-flight dispersion models: enforcing the well-mixed condition, *Journal of Applied Meteorology* **32**: 1695-1707.

Wilson, J.D., G.W. Thurtell, and G.E. Kidd, 1981: Numerical simulations of particle trajectories in inhomogeneous turbulence. III. Comparison of predictions with experimental data for the atmospheric surface layer, *Boundary-Layer Meteorology* **21**: 295-315.

Appendix A. Coordinate Rotation Scheme

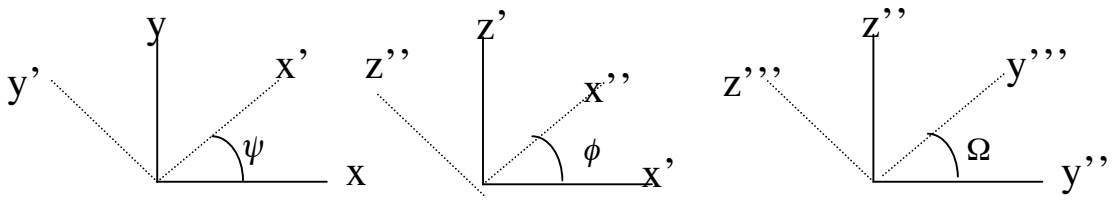

Fig. A1. The three rotations used in the wind-following coordinate system.

The random-walk code uses a local coordinate rotation scheme that occurs at each particle location x, y, and z. The x direction is aligned with the mean wind vector at the particle location, and the z direction is rotated into the direction of the strongest velocity gradient. The required axes rotations are shown above in Fig. A1.

The first rotation produces the x' and y' axis through rotation through the angle ψ where

$$\psi = \arctan\left(\frac{\overline{V}}{\overline{U}}\right).$$

The second rotation produces the x'' and z'' axes by rotation of the x' and z' axes through the angle ϕ where

$$\phi = \arctan\left(\frac{\overline{W}}{\sqrt{\overline{U}^2 + \overline{V}^2}}\right).$$

The third rotation produces the z''' and y''' axes from the z'' and y'' axes through rotation through the angle Ω. The angle Ω is calculated by maximizing the rate of change of the wind speed with respect to distance along the z''' axis,

$$\frac{\partial \overline{U}'''}{\partial z'''} = \frac{\partial s}{\partial x}\left(\sin\psi\sin\Omega - \cos\psi\sin\phi\cos\Omega\right) - \frac{\partial s}{\partial y}\left(\cos\psi\sin\Omega + \sin\psi\sin\phi\cos\Omega\right) + \frac{\partial s}{\partial z}\cos\phi\cos\Omega$$

with s the wind speed or $\overline{U}'''$. The optimization results in the equation:

$$\Omega = \arctan\left[\left(-\frac{\partial s}{\partial x}\sin\psi + \frac{\partial s}{\partial y}\cos\psi\right) \Big/ \left(\frac{\partial s}{\partial x}\cos\psi\sin\phi + \frac{\partial s}{\partial y}\sin\psi\sin\phi - \frac{\partial s}{\partial z}\cos\phi\right)\right]$$

which may result in a minimum rather than a maximum. If the above equation results in a minimum the appropriate value is found by replacing Ω with $\Omega + \pi$.

Unit vectors in the triply-rotated system are described by:

$$i_{x'''} = \cos\psi\cos\phi i_x + \sin\psi\cos\phi i_y + \sin\phi i_z,$$

$$i_{y'''} = -(\cos\psi\sin\phi\sin\Omega + \sin\psi\cos\Omega) i_x - (\sin\psi\sin\phi\sin\Omega - \cos\psi\cos\Omega) i_y - \cos\phi\sin\Omega i_z,$$

and,

$$i_{z'''} = (\sin\psi\sin\Omega - \cos\psi\sin\phi\cos\Omega) i_x - (\cos\psi\sin\Omega + \sin\psi\sin\phi\cos\Omega) i_y + \cos\phi\cos\Omega i_z.$$

We describe transformations from the rotated system to the unrotated system with the equations:

$$u = u'''\alpha_1 + v'''\alpha_2 + w'''\alpha_3,$$

$$v = u'''\beta_1 + v'''\beta_2 + w'''\beta_3,$$

and,

$$w = u'''\gamma_1 + v'''\gamma_2 + w'''\gamma_3,$$

where,

$$\alpha_1 = \cos\psi\cos\phi,$$

$$\alpha_2 = -\sin\psi\cos\Omega - \cos\psi\sin\phi\sin\Omega,$$

$$\alpha_3 = \sin\psi\sin\Omega - \cos\psi\sin\phi\cos\Omega,$$

$$\beta_1 = \sin\psi\cos\phi,$$

$$\beta_2 = \cos\psi\cos\Omega - \sin\psi\sin\phi\sin\Omega,$$

$$\beta_3 = -\cos\psi\sin\Omega - \sin\psi\sin\phi\cos\Omega,$$

$$\gamma_1 = \sin\phi,$$

$$\gamma_2 = \cos\phi\sin\Omega,$$

and,

$$\gamma_3 = \cos\phi\cos\Omega.$$

We describe the transformations from the unrotated system to the rotated system in a similar fashion:

$$u''' = u\alpha_{n1} + v\alpha_{n2} + w\alpha_{n3},$$

$$v''' = u\beta_{n1} + v\beta_{n2} + w\beta_{n3},$$

and,

$$w''' = u\gamma_{n1} + v\gamma_{n2} + w\gamma_{n3},$$

with,

$$\alpha_{n1} = \cos\psi\cos\phi,$$

$$\alpha_{n2} = \sin\psi\cos\phi,$$

$$\alpha_{n3} = \sin\phi,$$

$$\beta_{n1} = -\sin\psi\cos\Omega - \cos\psi\sin\phi\sin\Omega,$$

$$\beta_{n2} = \cos\psi\cos\Omega - \sin\psi\sin\phi\sin\Omega,$$

$$\beta_{n3} = \cos\phi\sin\Omega,$$

$$\gamma_{n1} = \sin\psi\sin\Omega - \cos\psi\sin\phi\cos\Omega,$$

$$\gamma_{n2} = -\cos\psi\cos\Omega - \sin\psi\sin\phi\cos\Omega,$$

and,

$$\gamma_{n3} = \cos\phi\cos\Omega.$$

Appendix B. Coordinate Rotation Scheme for Turbulence Parameters

The stresses obtained by this approach are appropriate to the mean wind, so that we have to transform the values into the original coordinate system. The relevant relationships are:

$$\omega = \arctan\left(\frac{v_{ls}}{u_{ls}}\right),$$

$$u = u_g \cos(\omega) + v_g \sin(\omega),$$

$$v = -u_g \sin(\omega) + v_g \cos(\omega),$$

$$\overline{u_f^2} = \overline{u_{gf}^2}\cos^2(\omega) + \bar{u}^2\cos^2(\omega) - 2\overline{u_{gf}v_{gf}}\cos(\omega)\sin(\omega) - 2\bar{u}\bar{v}\cos(\omega)\sin(\omega) + \overline{v_{gf}^2}\sin^2(\omega) + \bar{v}^2\sin^2(\omega) - \bar{u}^2,$$

$$\overline{v_f^2} = \overline{u_{gf}^2}\sin^2(\omega) + \bar{u}^2\sin^2(\omega) + 2\overline{u_{gf}v_{gf}}\cos(\omega)\sin(\omega) + 2\bar{u}\bar{v}\cos(\omega)\sin(\omega) + \overline{v_{gf}^2}\cos^2(\omega) + \bar{v}^2\cos^2(\omega) - \bar{v}^2$$

$$\overline{u_f v_f} = \overline{u_{gf}^2}\cos(\omega)\sin(\omega) + \bar{u}^2\cos(\omega)\sin(\omega) + \overline{u_{gf}v_{gf}}\left(\cos^2(\omega) - \sin^2(\omega)\right) + \bar{u}\bar{v}\left(\cos^2(\omega) - \sin^2(\omega)\right) - \overline{v_{gf}^2}\sin(\omega)\cos(\omega) - \bar{v}^2\sin(\omega)\cos(\omega) - \bar{u}\bar{v},$$

$$\overline{u_f w_f} = \overline{u_{gf}w_{gf}}\cos(\omega) + \bar{u}\bar{w}\cos(\omega) - \overline{v_{gf}w_{gf}}\sin(\omega) - \bar{u}\bar{w}\sin(\omega) - \overline{uw},$$

and,

$$\overline{v_f w_f} = \overline{u_{gf}v_{gf}}\sin(\omega) + \bar{u}\bar{w}\sin(\omega) + \overline{v_{gf}w_{gf}}\cos(\omega) + \bar{v}\bar{w}\cos(\omega) - \bar{v}\bar{w}.$$

With v_{ls}, the large scale v-component of the mean wind and u_{ls} the large scale u-component of the mean wind.

Turbulence Terms:

The parameterizations apply to the rotated coordinate system, but we also need to be able to describe the turbulent winds in the unrotated coordinate system. The above relationships can be used to describe the Reynolds stresses in the unrotated system in terms of the stresses and mean winds in the rotated system:

$$\overline{u_f^2} = \overline{u'''^2_f}\alpha_1^2 + s^2\alpha_1^2 + 2\overline{u'''_f v'''_f}\alpha_1\alpha_2 + 2\overline{u'''_f w'''_f}\alpha_1\alpha_3 + \overline{v'''^2_f}\alpha_2^2 + 2\overline{v'''_f w'''_f}\alpha_2\alpha_3 + \overline{w'''^2_f}\alpha_3^2 - \bar{u}^2,$$

$$\overline{v_f^2} = \overline{u'''^2_f}\beta_1^2 + s^2\beta_1^2 + 2\overline{u'''_f v'''_f}\beta_1\beta_2 + 2\overline{u'''_f w'''_f}\beta_1\beta_3 + 2\overline{v'''_f w'''_f}\beta_2\beta_3 + \overline{v'''^2_f}\beta_2^2 + \overline{w'''^2_f}\beta_3^2 - \bar{v}^2,$$

$$\overline{w_f^2} = \overline{u'''^2_f}\gamma_1^2 + s^2\gamma_1^2 + 2\overline{u'''_f v'''_f}\gamma_1\gamma_2 + 2\overline{u'''_f w'''_f}\gamma_1\gamma_3 + \overline{v'''^2_f}\gamma_2^2 + 2\overline{v'''_f w'''_f}\gamma_2\gamma_3 + \overline{w'''^2_f}\gamma_3^2 - \bar{w}^2,$$

$$\overline{u_f v_f} = \overline{u'''^2_f}\alpha_1\beta_1 + s^2\alpha_1\beta_1 + \overline{u'''_f v'''_f}(\alpha_1\beta_2 + \alpha_2\beta_1) + \overline{u'''_f w'''_f}(\alpha_1\beta_3 + \alpha_3\beta_1) + \overline{v'''^2_f}\alpha_2\beta_2 + \overline{v'''_f w'''_f}(\alpha_2\beta_3 + \alpha_3\beta_2) + \overline{w'''^2_f}\alpha_3\beta_3 - \bar{u}\bar{v},$$

$$\overline{u_f w_f} = \overline{u'''^2_f}\alpha_1\gamma_1 + s^2\alpha_1\gamma_1 + \overline{u'''_f v'''_f}(\alpha_1\gamma_2 + \alpha_2\gamma_1) + \overline{u'''_f w'''_f}(\alpha_1\gamma_3 + \alpha_3\gamma_1) + \overline{v'''^2_f}\alpha_2\gamma_2 + \overline{v'''_f w'''_f}(\alpha_2\gamma_3 + \alpha_3\gamma_2) + \overline{w'''^2_f}\alpha_3\gamma_3 - \bar{u}\bar{v},$$

and,

$$\overline{v_f w_f} = \overline{u'''^2_f}\beta_1\gamma_1 + s^2\beta_1\gamma_1 + \overline{u'''_f v'''_f}(\beta_1\gamma_2 + \beta_2\gamma_1) + \overline{u'''_f w'''_f}(\beta_1\gamma_3 + \beta_3\gamma_1) + \overline{v'''^2_f}\beta_2\gamma_2 + \overline{v'''_f w'''_f}(\beta_2\gamma_3 + \beta_3\gamma_2) + \overline{w'''^2_f}\beta_3\gamma_3 - \bar{v}\bar{w},$$

with the subscript f denoting a fluctuating or random component.

We use similar relationships to describe Reynolds stresses in the rotated system:

$$\overline{u'''^2_f} = \overline{u^2_f}\alpha^2_{n1} + \bar{u}^2\alpha^2_{n1} + 2\overline{u_f v_f}\alpha_{n1}\alpha_{n2} + 2\bar{u}\bar{v}\alpha_{n1}\alpha_{n2} + 2\overline{u_f w_f}\alpha_{n1}\alpha_{n3} + 2\bar{u}\bar{w}\alpha_{n1}\alpha_{n3} + \overline{v^2_f}\alpha^2_{n2} + \bar{v}^2\alpha^2_{n2} + 2\overline{v_f w_f}\alpha_{n2}\alpha_{n3} + 2\bar{v}\bar{w}\alpha_{n2}\alpha_{n3} + \overline{w^2_f}\alpha^2_{n3} + \bar{w}^2\alpha^2_{n3} - s^2,$$

$$\overline{v'''^2_f} = \overline{u^2_f}\beta^2_{n1} + \bar{u}^2\beta^2_{n1} + 2\overline{u_f v_f}\beta_{n1}\beta_{n2} + 2\bar{u}\bar{v}\beta_{n1}\beta_{n2} + 2\overline{u_f w_f}\beta_{n1}\beta_{n2} + 2\bar{u}\bar{w}\beta_{n1}\beta_{n2} + \overline{v^2_f}\beta^2_{n2} + \bar{v}^2\beta^2_{n2} + 2\overline{v_f w_f}\beta_{n2}\beta_{n3} + 2\bar{v}\bar{w}\beta_{n2}\beta_{n3} + \overline{w^2_f}\beta^2_{n3} + \bar{w}^2\beta^2_{n3},$$

$$\overline{w'''^2_f} = \overline{u^2_f}\gamma^2_{n1} + \bar{u}^2\gamma^2_{n1} + 2\overline{u_f v_f}\gamma_{n1}\gamma_{n2} + 2\bar{u}\bar{v}\gamma_{n1}\gamma_{n2} + 2\overline{u_f w_f}\gamma_{n1}\gamma_{n3} + 2\bar{u}\bar{w}\gamma_{n1}\gamma_{n3} + \overline{v^2_f}\gamma^2_{n2} + \bar{v}^2\gamma^2_{n2} + 2\overline{v_f w_f}\gamma_{n2}\gamma_{n3} + 2\bar{v}\bar{w}\gamma_{n2}\gamma_{n3} + \overline{w^2_f}\gamma^2_{n3} + \bar{w}^2\gamma^2_{n3},$$

and finally (the other shear stresses are not needed):

$$\overline{u'''_f w'''_f} = \overline{u^2_f}\alpha_{n1}\gamma_{n1} + \bar{u}^2\alpha_{n1}\gamma_{n1} + \overline{u_f v_f}(\alpha_{n1}\gamma_{n2} + \alpha_{n2}\gamma_{n1}) + \bar{u}\bar{v}(\alpha_{n1}\gamma_{n2} + \alpha_{n2}\gamma_{n1}) + \overline{u_f w_f}(\alpha_{n1}\gamma_{n3} + \alpha_{n3}\gamma_{n1}) + \bar{u}\bar{w}(\alpha_{n1}\gamma_{n3} + \alpha_{n3}\gamma_{n1}) + \overline{v^2_f}\alpha_{n2}\gamma_{n2} + \bar{v}^2\alpha_{n2}\gamma_{n2} + \overline{v_f w_f}(\alpha_{n2}\gamma_{n3} + \alpha_{n3}\gamma_{n2}) + \bar{v}\bar{w}(\alpha_{n2}\gamma_{n3} + \alpha_{n3}\gamma_{n2}) + \overline{w^2_f}\alpha_{n3}\gamma_{n3} + \bar{w}^2\alpha_{n3}\gamma_{n3}.$$

The equation for the dissipation remains:

$$\varepsilon = \frac{u_*^3}{k(d_{wall} + z_0)},$$

except that d_{wall} replaces z where d_{wall} is the smaller of z_{eff} and d_{wall}.

$$dw = -\frac{Co\varepsilon}{\lambda_3 w}dt + \frac{1}{2}\left(1 + \lambda_3 w^2\right)\frac{\partial \tau_{33}}{\partial w}dt + (Co\varepsilon dt)^{1/2}dW_3(t)$$